Modelling river runoff and estimating its weather-related uncertainty for 11 large-scale rivers located in different regions of the globe

Yeugeniy M. Gusev, Olga N. Nasonova, Evgeny E. Kovalev and Georgii V. Aizel

ABSTRACT

In order to study the possibility of reproducing river runoff with making use of the land surface model Soil Water–Atmosphere–Plants (SWAP) and information based on global data sets 11 river basins suggested within the framework of the Inter-Sectoral Impact Model Intercomparison Project and located in various regions of the globe under a wide variety of natural conditions were used. Schematization of each basin as a set of $0.5^\circ \times 0.5^\circ$ computational grid cells connected by a river network was carried out. Input data including atmospheric forcing data and land surface parameters based, respectively, on the global WATCH and ECOCLIMAP data sets were prepared for each grid cell. Simulations of river runoff performed by SWAP with a priori input data showed poor agreement with observations. Optimization of a number of model parameters substantially improved the results. The obtained results confirm the universal character of SWAP. Natural uncertainty of river runoff caused by weather noise was estimated and analysed. It can be treated as the lowest limit of predictability of river runoff. It was shown that differences in runoff uncertainties obtained for different rivers depend greatly on natural conditions of a river basin, in particular, on the ratio of deterministic and random components of the river runoff.

Key words | global data sets, ISI-MIP, parameters' calibration, physically based modelling, river runoff, weather-related uncertainty

Yeugeniy M. Gusev (corresponding author)
Olga N. Nasonova
Evgeny E. Kovalev
Georgii V. Aizel
Institute of Water Problems, Russian Academy of Sciences,
Gubkina St. 3,
Moscow 119333,
Russia
E-mail: *sowaso@yandex.ru*

INTRODUCTION

Simulating the dynamics of water balance components of river basins accounting for the processes of their formation is one of the main issues of modern hydrologic science. Observed and projected global climate change are motivating the scientific community towards the solution of this problem, forcing improvement of the existing methods and to look for new approaches for assessment and projection of river runoff and the other water balance components (Peel & Blöschl 2011). In spite of the fact that during the last 40 years there have been many attempts to create new hydrological models, which should be unique and universal, it can be stated that this problem has not been solved at the moment (Singh & Woolhiser 2000; Beven 2011).

This is also confirmed by the appearance of various international projects devoted to comparison of different hydrological models. One such project is the Inter-Sectoral Impact Model Intercomparison Project (ISI-MIP), launched in 2013 (Warszawski *et al.* 2013), the water sector of which is aimed at validation and improvement of hydrological models on regional and global scales and application of the models for hydrological projections of possible changes in water resources due to expected climate change. The

doi: 10.2166/nh.2017.015

authors of the present paper are participating in this project with their Soil Water–Atmosphere–Plants (SWAP) model (Gusev & Nasonova 2000; Gusev *et al.* 2006) and the results presented here were partly obtained within the framework of the second phase of the ISI-MIP (ISI-MIP2).

The SWAP model has been widely validated during the last two decades. As a rule, the validation was carried out using meteorological forcing data derived from observations at meteorological stations. However, such observations are not always available, do not cover the whole land surface of the Earth and represent point data. At the same time, there are many global data sets containing meteorological data at different temporal and spatial resolutions (e.g. Xu *et al.* 2016). That is why the first goal of the present work was investigating the ability of SWAP to reproduce runoff of rivers located in different regions of the globe under a wide variety of natural conditions (from areas with permafrost and severe arctic climate to humid areas of equatorial monsoons and arid regions of tropical and subtropical latitudes) using meteorological forcing data and land surface parameters derived from the global data sets suggested in the framework of the ISI-MIP2 project.

Similar large-scale multi-basin modelling studies were performed by nine hydrological models participating in the ISI-MIP. The summarized results can be found in the overview paper (Krysanova & Hattermann 2017).

Another important problem associated with hydrological simulation and projections is their inevitable uncertainties resulting from application of different climate and hydrological models, different greenhouse-gas emission scenarios, model parameters and so on. There are many publications devoted to estimation of these uncertainties, which should be taken into account at the stage of decision-making in water resource management and planning. Some of these uncertainties (epistemic ones) can be reduced, for example, due to obtaining new knowledge about climatic and hydrological systems, and improving the quality of models and data. However, there are also structural uncertainties which do not depend on our knowledge or data and are an inherent property of these systems. Such uncertainties cannot be reduced and should be treated as a lower limit of predictability in climatic or hydrological modelling (Gelfan *et al.* 2015). Considering river runoff, structural uncertainty of its simulations and projections is associated, in particular, with natural variability of runoff.

This variability, as shown in Gelfan *et al.* (2015) and Gusev *et al.* (2017), is caused by the chaotic nature of characteristics of atmospheric processes (so-called weather noise), their instability with respect to small changes in the initial conditions. The latter is confirmed by numerical experiments with atmosphere-ocean general circulation models (AOGCMs) when small errors in the initial conditions resulted in large scatter in simulations of the evolution of meteorological variables (see, for example, Gelfan *et al.* (2015)). In nature, differences in the initial state of the atmosphere (for example, at the beginning of each year), result from different (even very small) positions of the Earth on its path around the Sun, as well as the difference in the state of the atmosphere which has been forming during a previous period. Small changes in the initial state of the atmosphere (a nonlinear system with dissipation) lead to quite large changes in its further dynamics. This is one of the reasons that it is impossible to predict an actual dynamics of the climate system, because the initial conditions of the state of the atmosphere can never be prescribed with absolute accuracy.

The weather noise of atmospheric processes causes a corresponding noise of hydrological processes, resulting in natural uncertainty of hydrological variables (in particular, river runoff). This uncertainty can be treated as the lowest limit of predictability of river runoff, which means that further improvement of climatic, hydrological and land surface models (LSMs) cannot help one to obtain long-term hydrological projections with a lower uncertainty than this limit. Such estimates are of great interest because they provide an opportunity to compare changes in runoff due to climate change or man-made impacts with natural variability of river runoff (i.e., its variability in the case of stationary climate). In this context, the second goal of the present work was estimating and analysing the natural variability of river runoff caused by the weather noise.

STUDY AREA AND DATA

The selected river basins and their schematization

Eleven large-scale river basins selected in the ISI-MIP were used in the present study. They are situated in different

geographical zones in different continents (Figure 1) and include the Rhine and Tagus located in Europe, the Lena, Ganges, Upper Huanghe (Yellow), and Upper Yangtze in Asia, the Niger in Africa, the MacKenzie and Upper Mississippi in North America, the Upper Amazon in South America and the Darling in Australia. The areas of the basins range from 67,490 km^2 to 2,460,000 km^2 (Table 1). A description of the basins can be found in Krysanova & Hattermann (2017). Here, it should be noted that the basins substantially differ from one another by natural conditions (climatic, soil, vegetation, geomorphological, etc.) which is very important for the solution of the stated problems.

A spatial schematization of the river basins was derived from Wu *et al.* (2012). The basins are presented by a set of regular grid cells (with a spatial resolution $0.5^\circ \times 0.5^\circ$ in latitude and longitude) connected by a river network. The schemes of the selected river basins are shown in Figure A1 (available with the online version of this paper) and the number of computational grid cells for each basin is given in Table 1.

Meteorological forcing data

Meteorological forcing data needed to drive the SWAP model are the air temperature and humidity, precipitation, incoming fluxes of longwave and shortwave radiation, wind speed and air pressure. These data for each calculation grid cell of the selected basins for the period of 1970–2001 were derived from the Water and Global Change (WATCH) data set with $0.5^\circ \times 0.5^\circ$ spatial resolution (Weedon *et al.* 2011). WATCH was created on the basis of combining monthly values of ground-based measurements (including air temperature, the number of days with precipitation, cloudiness and precipitation) taken from the Global Precipitation Climatology Center (GPCC) and the Climatic Research Unit (CRU of University of East England) data sets, and the ERA-40 reanalysis data (with corrections to seasonal changes of atmospheric aerosols improving incoming solar radiation).

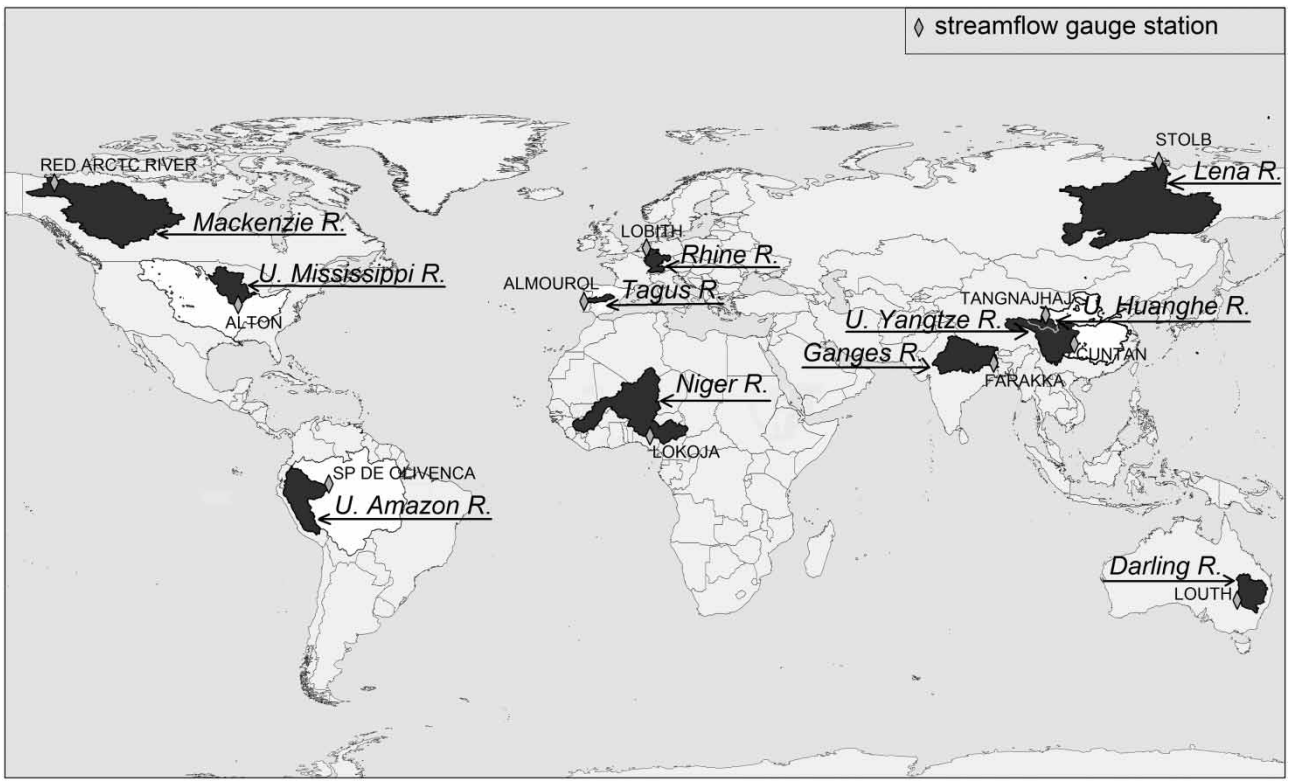

Figure 1 | The locations of the selected river basins.

Table 1 | River basins with their area and the number of calculational grid cells, gauge stations with their coordinates, averaged over 1971–2000 air temperature *T*, precipitation *P*, river runoff *R* and runoff ratio *R/P*

River	Streamflow gauge station	Latitude	Longitude	Area (km^2)	Number of grid cells	*T*, °C	*P*, mm/year	*R*, mm/year	*R/P*
Lena	Stolb	72.37	126.80	2,460,000	1,668	−10.2	384	201	0.52
U. Amazon	Sao Paulo de Olivenca	−3.45	−68.75	990,781	330	21.7	2,122	1,459	0.69
MacKenzie	Arctic Red River	67.46	−133.74	1,660,000	1,128	−4.3	435	171	0.39
U. Yangtze	Cuntan	29.61	106.60	804,859	325	6.8	768	389	0.51
Ganges	Farakka	25.00	87.92	835,000	340	21.1	1,173	471	0.4
U. Huanghe (Yellow)	Tangnaihai	35.50	100.15	121,000	51	−2	506	169	0.33
Niger	Lokoja	7.80	6.77	2,074,171	678	27.7	625	77	0.12
Rhine	Lobith	51.84	6.11	160,800	83	8.7	1,038	457	0.44
U. Mississippi	Alton	38.89	−90.18	444,185	198	7.3	967	257	0.27
Tagus	Almourol	39.47	−8.37	67,490	35	14	671	152	0.23
Darling	Louth	−30.53	145.11	489,300	180	19.2	590	8	0.01

The values of *T*, *P* and *R* are taken from Krysanova & Hattermann (2017).

Land surface parameters

Most vegetation parameters for the selected river basins were derived on the basis of the global ECOCLIMAP data set which has 1-km resolution and is based on classification including 215 ecosystems (Champeaux *et al.* 2005). The obtained parameters were aggregated by means of mosaic (tile) approach for each calculational grid cell.

As well, SWAP needs the following soil hydrophysical parameters: porosity, field capacity, wilting point, hydraulic conductivity at saturation, as well as soil matric potential at saturation and B-parameter in parameterization by Clapp & Hornberger (1978). These parameters were calculated by making use of equations given in Cosby *et al.* (1984) and data on soil texture (CLAY and SAND) taken from the ECOCLIMAP.

The obtained parameters were checked for consistency and some unrealistic values were corrected as proposed in Gusev *et al.* (2006).

Streamflow data

Streamflow data for the gauges listed in Table 1 were provided with a daily time step (with the exception of the Ganges, for which only monthly data were available) within the framework of the ISI-MIP2 project (see Huang *et al.* (2017) for details). Additional daily runoff data for subbasins of the Lena and MacKenzie rivers were taken from the the Global Runoff Data Centre (GRDC).

METHODS

SWAP model

The LSM SWAP is a physically based model describing heat and water exchange processes in a groundwater–soil water–vegetation/snow cover–near-surface atmosphere system (SVAS). The model treats the following processes: interception of liquid and solid precipitation by vegetation; evaporation, melting and freezing of intercepted precipitation, including refreezing of melt water; formation of snow cover at the forest floor and at the open site during the cold season; partitioning of non-intercepted precipitation or water yield of snow cover between surface runoff and infiltration into the soil; formation of the water balance of the aeration zone including transpiration, soil evaporation, water exchange with lower layers and dynamics of soil water storage; water table dynamics; formation of the heat balance and thermal regime of SVAS; soil freezing and thawing.

The SWAP model makes it possible to simulate the dynamics of heat and water balance components for terrestrial ecosystems and river basins on different scales and under different natural conditions. Spatial heterogeneity of

the territory is taken into account by application of the function of distribution of hydraulic conductivity at saturation (Gusev & Nasonova 1998). Different versions of SWAP and their validation have been detailed in a number of publications (e.g., Gusev & Nasonova 2000; Gusev *et al.* 2008, 2016a; Nasonova *et al.* 2009).

In hydrological applications, in the case of a grid box or a small catchment, a kinematic wave equation is used to simulate streamflow at the box/catchment outlet. Application of the SWAP model for a large-scale river basin requires schematization of the basin as a number of computational grid cells connected by a river network. Heat and water regimes are simulated independently for each grid cell. Runoff simulated for each cell is then transformed by a river routing model to obtain streamflow at the basin outlet. Here, a simple linear transfer model in river channels (Oki & Sud 1998) is used.

Participation of the SWAP model in numerous international projects, such as PILPS (phases 2a, 2c, 2d and 2e), Rhona-AGGregation, MOPEX, ALMIP-2 devoted to the comparative analysis of the quality of existing LSMs and hydrological models has shown that SWAP is able to reproduce the dynamics of water balance components and other hydrothermal characteristics of river basins quite adequately provided that input data of high quality are available (e.g., Wood *et al.* 1998; Gusev & Nasonova 2000; Boone *et al.* 2004; Nasonova *et al.* 2009; Getirana *et al.* 2017; Grippa *et al.* 2017).

Goodness-of-fit statistics

The agreement between simulated and observed streamflow for each river basin was estimated at monthly basis using several goodness-of-fit statistics: systematic error *Bias* (equalled to the difference between the simulated and observed mean values of river runoff):

$$Bias = \frac{\sum_{\Omega}(x_{cal} - x_{obs})}{\sum_{\Omega} x_{obs}} \cdot 100 \quad (1)$$

and the Nash and Sutcliffe coefficient of efficiency (Nash & Sutcliffe 1970) *NS* defined as follows:

$$NS = 1 - \frac{\sum_{\Omega}(x_{cal} - x_{obs})^2}{\sum_{\Omega}(x_{obs} - \bar{x}_{obs})^2}, \quad (2)$$

where x_{cal} and x_{obs} are calculated and observed values of a variable x (here, monthly river runoff), Ω is a discrete sample set of the variable x.

If $NS = 1$, the simulation is ideal. If $NS < 0$, temporal variability of variable x is reproduced poorly (in this case, a simple averaging of observations is better than model simulation). As to the *Bias*, it should be taken into account that it is desirable to reduce the error of runoff measurements to ~5% (WMO 1994) (this value may be much higher for flood periods). As such, the quality of runoff modelling can be considered as 'good' when $|Bias| \leq 5$–10%.

Calibration of model parameters

Parameters' calibration was carried out automatically using the algorithm for searching for the global extremum SCE-UA (Duan *et al.* 1992). The Nash and Sutcliffe efficiency was used as an objective function. The search for the maximum of the objective function was performed, as it was suggested in Nasonova *et al.* (2009), under the condition that an absolute value of the systematic error of simulation does not exceed 5%.

For the snow-dominated river basins (here, the Lena and MacKenzie), seven model parameters were calibrated: hydraulic conductivity at saturation, soil column thickness, rooting depth, albedo of vegetation in the warm period, albedo of snow cover, Manning's roughness coefficient, and the effective velocity of water movement in the channels (Gusev *et al.* 2008). For the rain-dominated rivers, the correcting factor for mean monthly leaf area index *LAI* was calibrated instead of albedo.

As previously mentioned, the forcing data were derived from the WATCH based on the reanalysis ERA-40 which may contain systematic errors as any product of reanalysis. To reduce the errors, the procedure of hybridization with monthly observations is often applied. In the WATCH, monthly measurements of precipitation were used for bias correction, while another important variable influencing runoff formation – incoming radiation – was not corrected. That is why in our study, correcting factors to incoming shortwave and longwave radiation were applied and calibrated (together with the model parameters) for all river basins (as in Gusev *et al.* 2008; Nasonova *et al.* 2009).

As well, to improve the results of calibration, the Lena and MacKenzie river basins were divided into three parts because of their large areas and optimal values of

parameters were obtained for each part. As shown in Gusev *et al.* (2016a, 2016b), such a division allows the improvement of the quality of simulations.

Calibration was performed for eight years (different for different rivers depending on available measured runoff); the rest of the years were used for model validation with the exception of the Tagus and Ganges rivers for which all available measured runoff (during eight and four years, respectively) was used for calibration.

Technique for estimation and analysis of natural river runoff uncertainty

Here, we used the following index *Un* (suggested in Gusev *et al.* (2017)) as the uncertainty measure of a positive variable X with a random component:

$$Un = \frac{(x_{0.975} - x_{0.025})}{M(X)}, \tag{3}$$

where $x_{0.975}$ and $x_{0.025}$ are the 97.5% and 2.5% quantiles for X, $M(X)$ is the estimate of the mean value. This index is the ratio of the interval, where a random quantity can appear with the 95% probability, to its mean value. Hereinafter, *Un* will be named as a relative uncertainty of X to distinguish it from an absolute uncertainty: $Un_{abs} = (x_{0.975} - x_{0.025})$.

In order to analyse the differences in runoff uncertainties obtained for different rivers, the spectral analysis which is widely used both in technical fields and in atmospheric sciences (Coley & Tukey 1965; Panofsky & Brier 1968; Belotserkovskii 1993) was applied. In hydrology, the spectral decomposition of the water balance components (precipitation, evapotranspiration and river runoff) was performed and analysed in Gusev *et al.* (2017).

Since natural uncertainty of river runoff is associated with its stochastic component (weather noise), one can try to determine, as the first approximation, the ratio of a regular component of runoff to a stochastic one. For this purpose, the expansion of a temporal evolution of river runoff into the Fourier series can be used. Since any variable (both deterministic and random) can be represented as the sum of harmonic oscillations (Fourier series), this procedure was carried out for an annual course of runoff of the rivers under study and spectral densities S of daily river runoff were calculated for harmonics with different frequencies f. For this purpose, the measured values of daily runoff were used for all rivers except for the Ganges River, for which daily measurements were not available. In this case, the simulated daily runoff was used.

Figure 2 shows a typical spectral density S of river runoff for harmonics with different frequencies f (Gusev *et al.* 2017).

As can be seen in Figure 2, the spectral density of river runoff has a clearly pronounced maximum at the frequency $f_{an} = 2.738 \times 10^{-3}$ day^{-1} (marked with the number 1), which corresponds to a temporal period of one year. This situation is obvious due to the rotation of the Earth around the Sun with an annual period, and the component $S(f_{an})$ as well as components which are close to it in frequency (as Hamming window was used for the calculation of S 'to involve a trade-off between resolving comparable strength components with similar frequencies and resolving disparate strength components with dissimilar frequencies' (Harris 1978)) are regular deterministic components of $S(f)$. As well, there may be other peaks corresponding to periods T/n, where $T = 1$ year, n = 2, 3, … (marked with the numbers 2 and 3 in Figure 2). In particular, the second peak corresponds to a semiannual period and so on. All these peaks are caused by deterministic reasons, for example, by influence of spring flood, monsoon rain period, etc. However, the most important thing is that the function $S(f)$ has a

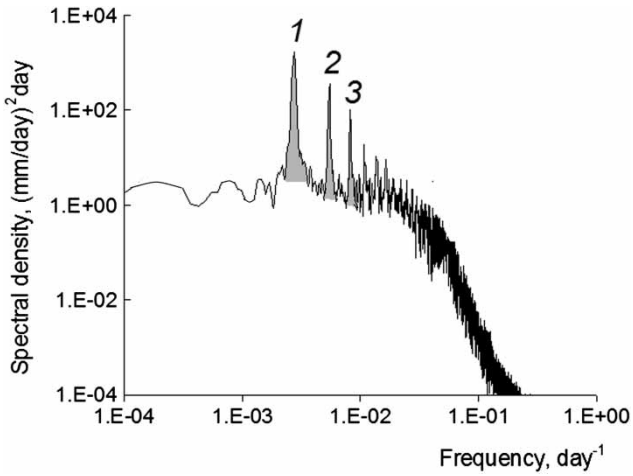

Figure 2 | A typical spectral density of daily river runoff.

maximum f_{an}. The value of $S(f_{an})$ was chosen as an indicator of the contribution of deterministic components into the spectral density $S(f)$.

Random fluctuations of river runoff caused by the weather noise also contribute to fluctuations of the spectral functions. An index reflecting the contribution of random components of runoff was created as follows. The largest peaks (usually 1–3, see Figure 2) of $S(f)$ were 'cut off' to remove the most significant part of the regular component. It should be noted that the number of peaks can be increased; however, it was found that cutting off further peaks, as a rule, has little effect on the final result. Then, for the transformed function $S(f)$, the standard deviation σ_s caused primarily by the weather noise was calculated. Note that values of $S(f)$ at frequencies larger than 0.03–0.1 (when $S(f)$ sharply decreases) do not make a significant contribution to σ_s-values.

Thus, two quantities related to the regular component of river runoff and to its stochastic component caused by the weather noise were obtained: $S(f_{an})$ and σ_s, respectively. They can be used for constructing *RSR*-criterion (regularity-to-stochasticity ratio):

$$RSR = \frac{S(f_{an})}{\sigma_s}, \tag{4}$$

which reflects the relationship between regular and stochastic components of river runoff. Evidently, the larger *RSR*-value the more regular runoff is.

It should be noted that the suggested criterion reflects this relationship approximately, because it is based on the data of only one random realization (occurred in nature) of the dynamics of river runoff (out of a large number of potentially possible realizations). Nevertheless, it can be used as the first approximation that is confirmed by the obtained good agreement between the uncertainty of river runoff and the proposed criterion (see below).

RESULTS AND DISCUSSION

Streamflow simulations

At the first stage SWAP was run using meteorological forcing data and land surface parameters derived, respectively, from the WATCH and ECOCLIMAP data sets and called a priori input data. Simulations were carried out with a daily time step for the period of 1970–2001. The simulated runoff was compared with measurements for different periods depending on the availability of measurements.

Application of a priori model parameters resulted in a poor agreement between measured and simulated monthly river runoff: for most basins $NS < 0$, *Bias* ranged from 3% (for the Upper Mississippi) to 340% (for the Darling) (Table 2).

Calibration of the parameters resulted in substantial improvement of model performance. Figure 3 illustrates the ability of SWAP to reproduce monthly hydrographs of rivers located under contrasting natural conditions: for the Upper Amazon (with the largest runoff R and runoff ratio R/P equalled to 1,460 mm/year and 0.69, respectively), Darling (with the lowest R and R/P equalled, respectively, to 8 mm/year and 0.01) and MacKenzie (with the negative mean annual air temperature and $R/P = 0.39$, the latter is close to the average value among the 11 rivers).

Figure 4 provides mean monthly hydrographs for all the rivers simulated by SWAP with a priori and optimized parameters. Comparison of both model runs with measured runoff shows that calibration of model parameters substantially improved the quality of simulations. This is also confirmed by goodness-of-fit statistics given in Table 2 for the calibration and the whole simulation periods. As can be seen, for the calibration period, absolute value of *Bias* does not exceed 5.1% (mean value is 2.4%), *NS* coefficient ranges from 0.68 to 0.95 (mean value is 0.85). For the whole period, absolute *Bias* is lower than 13.8% with a mean value of 4.4%, NS-values are within the interval of 0.58–0.90 with a mean value of 0.78. The obtained results can be treated as good for all the rivers with the exception of the Lena, for which the quality of runoff simulations is the lowest and can be treated only as satisfactory. This can be explained by the lower quality of meteorological forcing data for the Lena River basin. In Gusev *et al.* (2016a), where forcing data were derived from measurements at meteorological stations located within the Lena basin, the quality of simulation of monthly river runoff was much higher in terms of NS ($NS = 0.93$), in spite of a coarser spatial resolution ($1^\circ \times 1^\circ$).

Table 2 | Systematic error (*Bias*) and Nash–Sutcliffe coefficient of efficiency (*NS*) for monthly values of river runoff simulated using the model SWAP with a set of a priori and calibrated model parameters, as well as relative uncertainties of annual and monthly river runoff

		A priori parameters			Calibrated parameters							
					Calibration period			Validation period				
River	Streamflow gauge station	Years	*Bias*, %	*NS*	Years	*Bias*, %	*NS*	Years	*Bias*, %	*NS*	Uncertainty of annual runoff	Mean uncertainty of monthly runoff
Lena	Stolb	1970–2001	8.5	0.44	1972–1979	0.2	0.68	1970–2001	−0.5	0.58	0.40	2.00
U. Amazon	Sao Paulo de Olivenca	1973–2001	−28.0	−0.22	1976–1983	−0.1	0.85	1973–2001	−1.1	0.82	0.41	0.59
MacKenzie	Arctic Red River	1970–2001	−26.1	−0.68	1973–1980	−1.1	0.83	1970–2001	2.8	0.76	0.42	0.65
U. Yangtze	Cuntan	1971–2001	−30.5	−0.30	1973–1980	−1.1	0.95	1971–2001	2.4	0.90	0.44	0.90
Ganges	Farakka	1970–1973	37.7	0.22	1970–1973	−5.0	0.93	–	–	–	0.74	1.47
U. Huanghe	Tangnaihai	1971–2001	−49.9	−0.10	1973–1980	−4.0	0.87	1971–2001	3.1	0.74	0.82	1.06
Niger	Lokoja	1970–2001	206.1	−7.90	1972–1979	−5.1	0.88	1970–2001	−13.8	0.85	0.87	1.27
Rhine	Lobith	1971–2001	29.1	−1.44	1975–2001	2.9	0.74	1971–2001	−1.9	0.74	1.00	1.80
U. Mississippi	Alton	1971–1987	2.9	−0.05	1973–1982	−4.6	0.82	1971–1987	−3.4	0.75	1.20	1.90
Tagus	Almourol	1983–1990	68.4	−0.08	1983–1990	−1.4	0.90	–	–	–	2.10	3.80
Darling	Louth	1970–2001	343.0	−6.50	1972–1979	−1.5	0.92	1970–2001	11.0	0.85	4.40	4.40

Nevertheless, in general, for all the rivers the specific features of river runoff are reproduced quite adequately, although the rivers are situated in different natural conditions with respect to both climate (from arctic to equatorial and from arid to humid) and soil/vegetation (from unfrozen and seasonally frozen soils to permafrost, as well as from tundra to subtropical forests).

Estimation of river runoff uncertainty caused by the weather noise

Figure 5 shows averaged over the simulation period annual runoff for the 11 rivers and the boundaries of its natural variation (absolute uncertainty Un_{abs}), as well as annual values of measured runoff for the same period. The values of uncertainty of annual runoff were estimated under the assumption that the probability distribution of annual runoff can be approximated by a log-normal distribution function. As can be seen in Figure 5, the measurements are within the range of uncertainty with 95% probability for all rivers. This is also confirmed by the results obtained for monthly runoff. Figure 6 shows the modelled hydrographs averaged over the simulation periods, the ranges of their absolute uncertainties and monthly runoff measured in different years.

Relative uncertainties of annual and monthly runoff are given in Table 2. As can be seen, monthly uncertainties for all rivers are higher than the annual ones. The reason is that for the greater averaging intervals, the multidirectional deviations of a variable from its mean value are mutually compensated, resulting in a decrease in the relative scatter of the values.

As well, analysis of the obtained results shows that uncertainties of river runoff largely depend on natural conditions of a river basin. In particular, they depend on the degree of determinism of the annual course of river runoff. The lowest uncertainty of annual runoff corresponds to the rivers with a clearly pronounced annual course of their runoff. Thus, the northern rivers (the Lena and Mackenzie) with a snow-dominated feeding and clearly pronounced spring flood have relatively low values of runoff uncertainty. The Upper Amazon is also characterized by a relatively small uncertainty because snow feeding also plays an important role in this part of the river basin. In addition, some smoothing of runoff hydrograph of the Upper Amazon occurs due to the fact that its

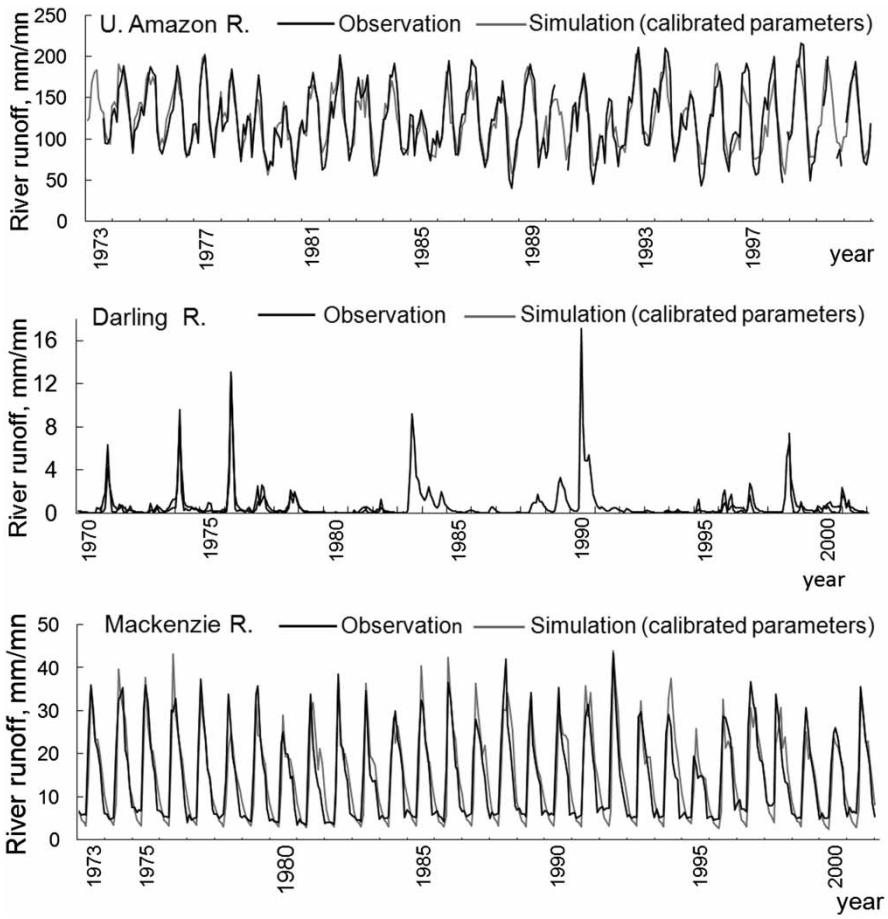

Figure 3 | Comparison of river runoff measured and simulated by the SWAP model with calibrated parameters for the Upper Amazon, Darling and Upper MacKenzie rivers (for gauges listed in Table 1).

right tributaries are located in the southern hemisphere, while the left tributaries are in the northern one. The Niger, Ganges, Yangtze and Huanghe rivers with more or less pronounced periodical impact of summer monsoon have slightly higher uncertainty of runoff compared to the rivers with a distinct spring flood peak.

Further increase in runoff uncertainty was found for the Rhine and Upper Mississippi rivers which are characterized by a mixed feeding (both snow and rain). The annual course of precipitation is smoothed in the Mississippi basin and absent in the Rhine basin (see Figure 2 in Krysanova & Hattermann (2017)). In addition, these rivers (especially the Rhine) do not have a clearly pronounced spring flood every year. This means that the contribution of regular components to runoff formation is lower compared to the above seven rivers.

Finally, the Tagus and Darling, being the rain-dominated rivers, have the highest uncertainty of river runoff. The climate in the Tagus basin is Mediterranean with a strong continental influence. Not only monthly, but also annual precipitation varies greatly in space and time. As to the Darling, the climate in the basin can be treated as tropical desert, and the river is supplied with water very irregularly. The Darling's numerous tributaries have their sources in the arid part of Australia, and many of them reach the main river only during occasional periods of flood. In the dry season, the river becomes much shallower or dries up. Nevertheless, in summer (although rarely), the river can cause damaging floods due to the climate and orography of the area. This results in the highest uncertainty in the Darling's runoff (Table 2).

The above considered qualitative analysis of the relationship between the uncertainty of river runoff and

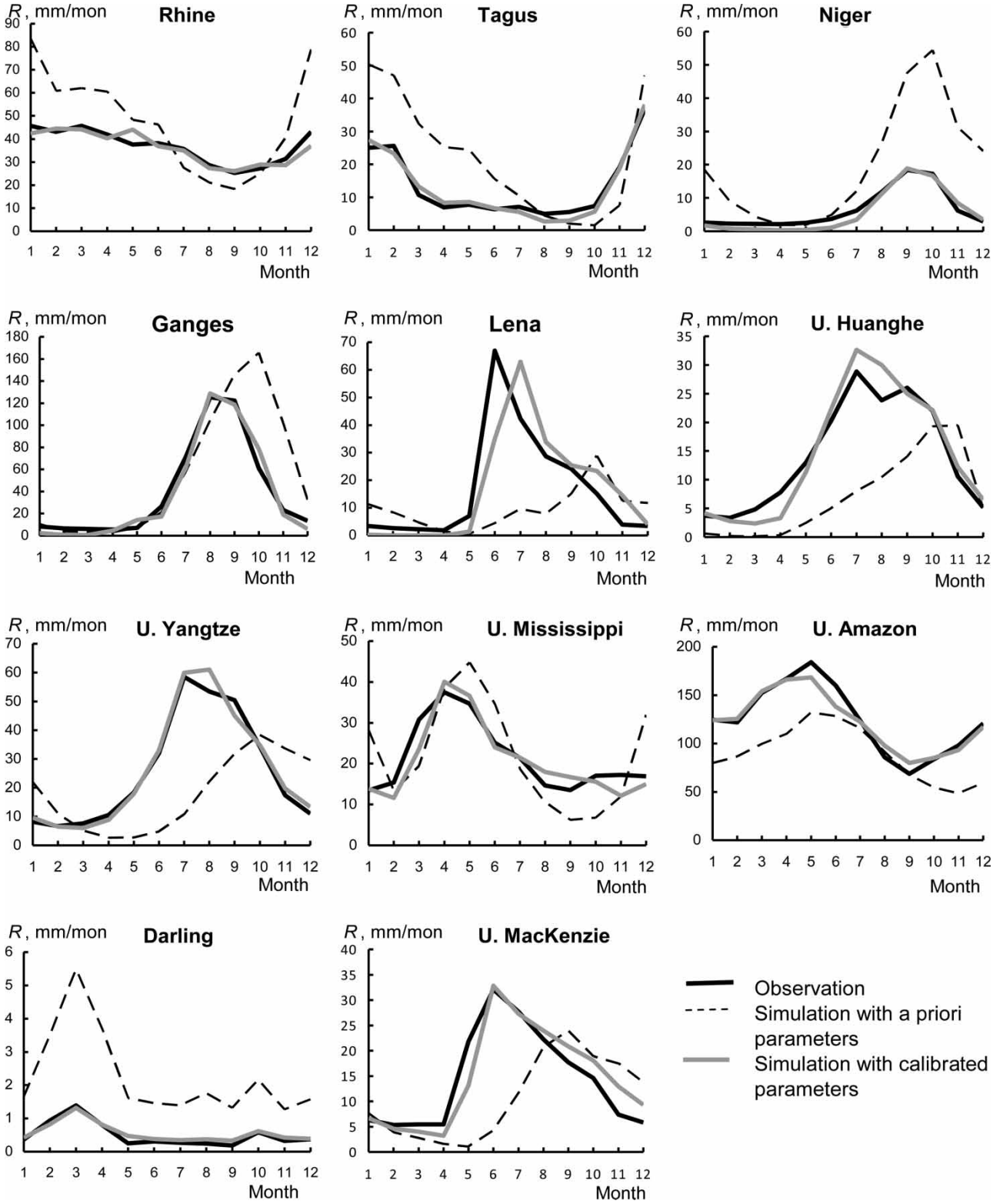

Figure 4 | Many-year averaged monthly hydrographs for 11 rivers measured at the basin outlets (black line) and simulated by the SWAP model with a priori parameters (dashed black line) and with calibrated parameters (grey line).

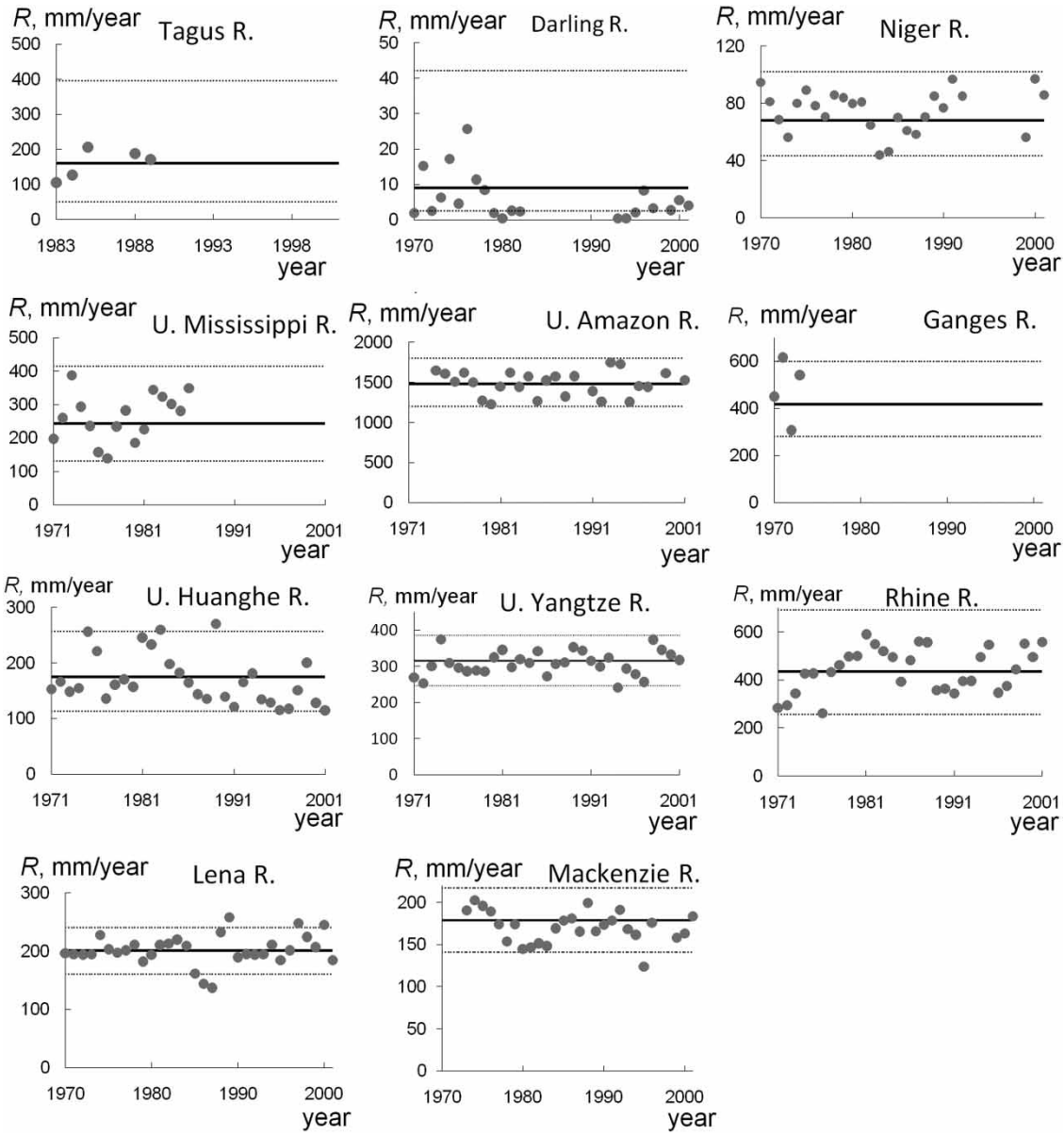

Figure 5 | Natural (weather related) uncertainty Un_{abs} of annual runoff R of the 11 rivers. Bold black line is the simulated annual runoff averaged over the simulation period; dashed lines (corresponding to the 97.5% and 2.5% quantiles for R) mark the interval of absolute uncertainty of annual runoff; grey circles are measured annual runoff.

the ratio of its regular and stochastic components can be illustrated quantitatively using the above described technique for spectral decomposition of the dynamics of river runoff. Figure 7 shows examples of the spectral densities $S(f)$ of daily runoff for the Upper Yangtze, Lena and Darling rivers characterized by different climatic conditions. The spectral densities for the other rivers are given in Figure A2 (available with the online version of this paper).

As can be seen in Figure 7, the spectral density of river runoff of the Lena and Yangtze has, as was expected, a clearly pronounced maximum at a frequency $f_{an} = 2.738 \times 10^{-3}$ day^{-1} (marked with the number 1) corresponding to a temporal period of one year. Such a maximum is absent for the Darling River. This will be explained below.

When analysing the spectral densities of runoff for the 11 rivers (including those listed in Figure A2), it can be

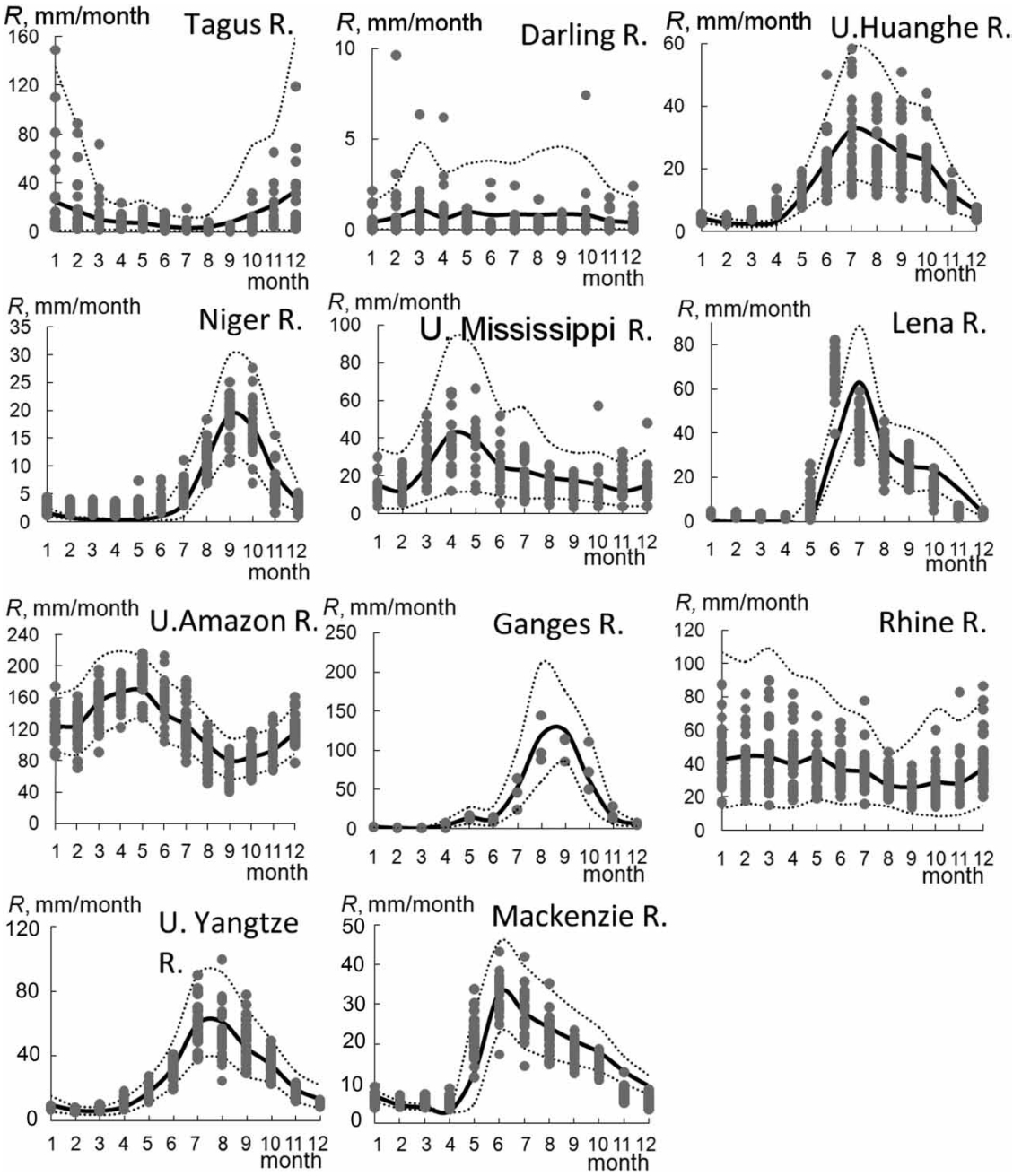

Figure 6 | Natural (weather related) uncertainty of monthly runoff *R* of the 11 rivers. Bold black line is averaged hydrograph of simulated monthly runoff; dotted lines (corresponding to the 97.5% and 2.5% quantiles for monthly *R*) show the interval of uncertainty of monthly runoff; grey circles are measured monthly runoff in different years.

seen that the spectral density does not have an annual peak only for the Darling and Tagus rivers. This means that in these cases a regular component has a small effect on runoff formation. For the remaining rivers, the highest peaks are mainly at the frequencies corresponding to the annual and semiannual periods. The rivers with a clearly pronounced spring flood or the monsoon character of precipitation (the Lena, Mackenzie, Upper Amazon, Upper Yangtze, Upper Huanghe, Niger and Ganges) have, as a rule, the largest amplitude of the main peaks. The Upper

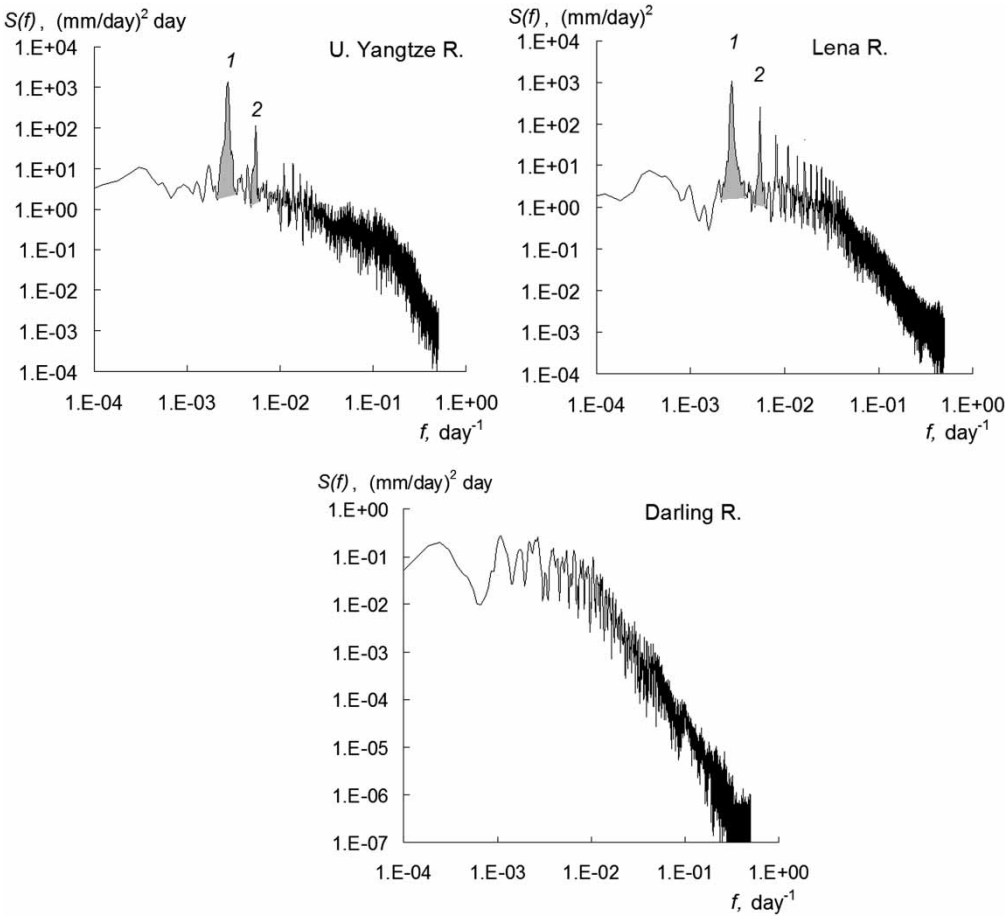

Figure 7 | Spectral densities of daily runoff for the basins of the Upper Yangtze, Lena and Darling rivers. The numbers 1 and 2 mark the major peaks of the spectral densities which correspond to annual and semiannual harmonics under the expansion of a temporal evolution of runoff into the Fourier series. Grey colour marks 'cut off' parts of spectral densities (see explanation in the text).

Mississippi and Rhine rivers also have peaks 1 and 2, but their amplitude is smaller than for the above-mentioned group of rivers and these two rivers have an intermediate position between the group of the above seven rivers and the Darling and Tagus rivers. All that has been said is vividly confirmed by Figure 7.

Figure 8 shows the relationship between *RSR* and uncertainty of annual runoff Un_{an} (Figure 8(a)) or mean uncertainty of monthly runoff $Un_{mn,aver}$ (Figure 8(b)). The obtained dependencies show that when the regular component in runoff formation increases the river runoff uncertainty becomes lower both on annual and monthly scales. Thus, Figure 8 is in good agreement with the above qualitative analysis of the dependence of runoff uncertainties for different rivers on the annual periodicity of runoff formation.

The most outstanding river is the Darling. As mentioned above, the spectral density of runoff $S(f)$ for the Darling River does not have a maximum at the frequency f_{an} (nevertheless, for the numerator in the *RSR* criterion, the value of $S(f_{an})$ was used). Such a situation is extremely rare and occurs only in the case of very strong stochasticity. In Figure 8, it is clearly seen that the Darling has the lowest value of *RSR*, i.e., its flow is characterized by an extremely high degree of stochasticity. In fact, the Darling River flow is known to be very irregular. Its numerous tributaries have sources in the arid inner part of Australia, and many of them reach the main watercourse only in occasional periods of flood. In the dry season, the river in its lower course dries up and breaks up into separate river parts. During a drought, which sometimes lasts more than a

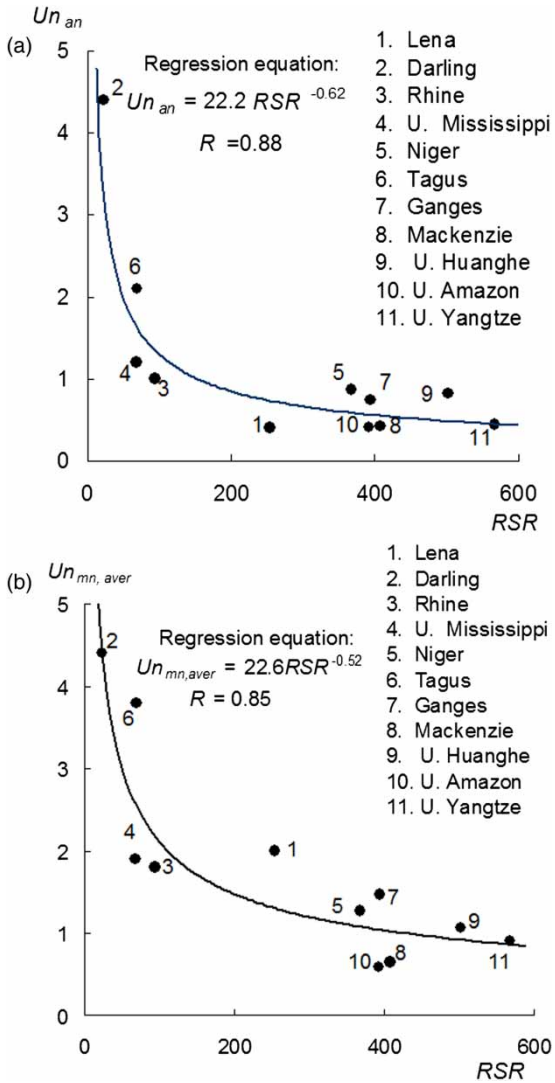

Figure 8 | Dependence of uncertainty of annual runoff Un_{an} (a) and averaged uncertainty of monthly runoff $Un_{mn,aver}$ (b) on the *RSR*-criterion (regularity-to-stochasticity ratio) for the 11 rivers under study.

year, the Darling becomes much shallower, transforming into a stunted brook. However, although rare, in summer the river can become damaging.

CONCLUSIONS

The simulations of streamflow of 11 rivers with a priori input data including meteorological variables and land surface parameters derived from the global WATCH and ECOCLIMAP data sets were performed using the SWAP model. The simulated river runoff showed poor agreement with measurements, motivating calibration of model parameters influencing runoff formation to the most extent. Calibration of selected parameters (including correcting factors to incoming radiation) for all river basins was performed against measured values of monthly runoff for several years. Application of the calibrated parameters substantially improved the results. Thus, for the validation period, the coefficient of efficiency for nine rivers ranged from 0.58 to 0.9 (averaged to 0.78), while mean absolute bias was within the range from 0.5% to 13.8% (averaged to 4.4%).

Analysis of the obtained results shows that simulation of river runoff by the SWAP model in combination with input data derived from the global WATCH and ECOCLIMAP data sets can be considered (after calibration of the most influencing parameters) as fairly good for river basins located under different natural conditions. This conclusion is of great importance because meteorological observations and land surface parameters are not available for many regions of the globe and in such cases global data sets may be the only source of information for hydrological calculations.

Natural variability of river runoff caused by the impact of weather noise (associated with a chaotic character of atmospheric processes resulting in stochastic instability of meteorological characteristics of near-surface layer of the atmosphere and determining the lowest limit of uncertainty in the estimates of meteorological variables simulated by climatic models) was estimated on two time scales (annual and monthly) for the selected rivers. This uncertainty can be treated as the lowest limit of predictability of river runoff.

Analysis of the estimated uncertainties has revealed that monthly uncertainties of river runoff are larger than annual ones. In addition, it was shown that differences in runoff uncertainties obtained for different rivers depend greatly on natural conditions of a river basin, in particular, on the ratio of deterministic and random components of the river runoff formation.

The obtained values of natural uncertainty of both annual river runoff and climatic hydrographs, as well as the dependencies of the uncertainties on regularity-to-stochasticity ratio can be used for comparison with possible

values of projected changes in annual and monthly runoff due to climate change and increasing impact of human activity. This study creates a sound basis for application of climate scenarios and projecting the dynamics of river runoff for the selected river basins by the end of the 21st century.

ACKNOWLEDGEMENTS

The work was supported by the Russian Science Foundation, project no. 16-17-10039. River runoff data were kindly provided by ISI-MIP organizers and the Global Runoff Data Centre (GRDC), D-56068 Koblenz, Germany.

REFERENCES

Belotserkovskii, A. V. 1993 *Spectral Analysis in Hydrometeorology*. Tutorial. RGGMI, Leningrad (in Russian).

Beven, K. 2011 Distributed models and uncertainty in flood risk management. In: *Flood Risk Science and Management* (G. Pender & H. Faulkner, eds). Wiley-Blackwell, Oxford, UK, pp. 291–312. doi: 10.1002/9781444324846.ch14.

Boone, A., Habets, F., Noilhan, J., Clark, D., Dirmeyer, P., Fox, S., Gusev, Y., Haddeland, I., Koster, R., Lohmann, D., Mahanama, S., Mitchell, K., Nasonova, O., Niu, G.-Y., Pitman, A., Polcher, J., Shmakin, A. B., Tanaka, K., van den Hurk, B., Verant, S., Verseghy, D., Viterbo, P. & Yang, Z.-L. 2004 The Rhone-aggregation land surface scheme intercomparison project: an overview. *Journal of Climate* **17** (1), 187–208. doi: 10.1175/1520-0442(2004)017 < 0187: TRLSSI > 2.0.CO;2.

Champeaux, J. L., Masson, V. & Chauvin, F. 2005 ECOCLIMAP: a global database of land surface parameters at 1 km resolution. *Meteorological Applications* **12** (1), 29–32. doi: 10.1017/S1350482705001519.

Clapp, R. B. & Hornberger, G. M. 1978 Empirical equations for some soil hydraulic properties. *Water Resources Research* **14** (4), 601–604. doi: 10.1029/WR014i004p00601.

Coley, J. W. & Tukey, J. W. 1965 An algorithm for the machine calculation of complex Fourier series. *Mathematics of Computation* **19**, 297–301. doi: https://doi.org/10.1090/S0025-5718-1965-0178586-1.

Cosby, B., Hornberger, G., Clapp, R. & Ginn, T. 1984 A statistical exploration of the relationships of soil moisture characteristics to the physical properties of soils. *Water Resources Research* **20** (6), 682–690. doi: 10.1029/WR020i006p00682.

Duan, Q., Sorooshian, S. & Gupta, V. K. 1992 Effective and efficient global optimization for conceptual rainfall runoff models. *Water Resources Research* **28** (4), 1015–1031.

Gelfan, A., Semenov, V. A., Gusev, E., Motovilov, Y., Nasonova, O., Krylenko, I. & Kovalev, E. 2015 Large-basin hydrological response to climate model outputs: uncertainty caused by the internal atmospheric variability. *Hydrology and Earth System Sciences Discussions* **19** (6), 2737–2754. doi: 10.5194/hess-19-2737-2015.

Getirana, A., Boone, A., Peugeot, C. & the ALMIP-2 Working Group. 2017 Streamflows over a West African basin from the ALMIP-2 model ensemble. *Journal of Hydrometeorology*. doi: 10.1175/JHM-D-16-0233.1.

Grippa, M., Kergoat, L., Boone, A., Peugeot, C., Demarty, J., Cappelaere, B., Gal, L., Hiernaux, P., Mougin, E., Ducharne, A., Dutra, E., Anderson, M. & Hain, C.. 2017 Modelling surface runoff and water fluxes over contrasted soils in pastoral Sahel: evaluation of the ALMIP2 land surface models over the Gourma region in Mali. *J. Hydrometeor.* doi: 10.1175/JHM-D-16-0170.1.

Gusev, Y. M. & Nasonova, O. N. 1998 The land surface parameterization scheme SWAP: description and partial validation. *Global and Planetary Change* **19** (1–4), 63–86.

Gusev, Y. M. & Nasonova, O. N. 2000 An experience of modelling heat and water exchange at the land surface on a large river basin scale. *Journal of Hydrology* **233** (1), 1–18. doi: 10.1016/S0022-1694(00)00225-0.

Gusev, E. M., Nasonova, O. N. & Kovalev, E. E. 2006 Modeling the components of heat and water balance for the land surface of the globe. *Water Resources* **33** (6), 616–627. doi: 10.1134/S0097807806060030.

Gusev, E. M., Nasonova, O. N., Dzhogan, L. Y & Kovalev, E. E. 2008 The application of the land surface model for calculating river runoff in high latitudes. *Water Resources* **35** (2), 171–184. doi: 10.1134/S009780780802005X.

Gusev, E. M., Nasonova, O. N. & Dzhogan, L. Y. 2016a Physically based modeling of many-year dynamics of daily streamflow and snow water equivalent in the Lena R basin. *Water Resources* **43** (1), 21–32. doi: 10.1134/S0097807816010085.

Gusev, E. M., Nasonova, O. N. & Dzhogan, L. Y. 2016b Scenario prediction of changes in water balance components in the Lena Basin in the context of possible climate changes. *Water Resources* **43** (5), 754–765. doi: 10.1134/S0097807816050079.

Gusev, Y. M., Semenov, V. A., Nasonova, O. N. & Kovalev, E. E. 2017 Climate noise impact on the uncertainty of simulated water balance components of river basins. *Hydrological Sciences Journal* **62** (8), 1181–1199. doi: 10.1080/02626667.2017.131906.

Harris, F. J. 1978 On the use of windows for harmonic analysis with the discrete Fourier transform. *Proceedings of the IEEE* **66** (1), 51–83. doi: 10.1109/PROC.1978.10837.

Huang, S., Kumar, R., Florke, M., Yang, T., Hundecha, Y., Kraft, P., Gao, C., Gelfan, A., Liersch, S., Lobanova, A., Strauch, M., Ogtrop, F., Reinhardt, J., Haberlandt, U. & Krysanova, V.

2017 Evaluation of an ensemble of regional hydrological models in 12 large-scale river basins worldwide. *Climatic Change* **141** (3), 381–397. doi: 10.1007/s10584-016-1841-8.

Krysanova, V. & Hattermann, F. 2017 Intercomparison of climate change impacts in 12 large river basins: overview of methods and summary of results. *Climatic Change* **141** (3), 363–379. doi: 10.1007/s10584-017-1919-y.

Nash, J. E. & Sutcliffe, J. V. 1970 River flow forecasting through conceptual models: 1. A discussion of principles. *Journal of Hydrology* **10** (3), 282–290. doi: 10.1016/0022-1694(70)90255-6.

Nasonova, O. N., Gusev, Y. M. & Kovalev, Y. E. 2009 Investigating the ability of a land surface model to simulate streamflow with the accuracy of hydrological models: a case study using MOPEX materials. *Journal of Hydrometeorology* **10** (5), 1128–1150. doi: 10.1175/2009JHM1083.1.

Oki, T. & Sud, Y. C. 1998 Design of total runoff integrating pathways (TRIP) – a global river channel network. *Earth Interactions* **2** (1), 1–37. doi: 10.1175/1087-3562(1998)002 < 0001:DOTRIP > 2.3.CO;2.

Panofsky, H. A. & Brier, G. W. 1968 *Some Applications of Statistics to Meteorology*. University Park, Pennsylvania.

Peel, M. C. & Blöschl, G. 2011 Hydrologic modelling in a changing world. *Progress in Physical Geography* **35** (2), 249–261. doi: 10.1177/0309133311402550.

Singh, V. P. & Woolhiser, D. A. 2000 Mathematical modeling of watershed hydrology. *Journal of Hydrologic Engineering* **7** (4), 270–292. doi: 10.1061/(ASCE)1084-0699(2002)7:4(270).

Warszawski, L., Frieler, K., Huber, V., Piontek, F., Serdeczny, O. & Schewe, J. 2013 The Inter-Sectoral Impact Model Intercomparison Project (ISI–MIP): project framework. *Proceedings of the National Academy of Sciences* **111** (9), 3228–3232. doi: 10.1073/pnas.1312330110.

Weedon, G. P., Gomes, S., Viterbo, P., Shuttleworth, W. J., Blyth, E., Österle, H., Adam, J. C., Bellouin, O. & Best, M. 2011 Creation of the WATCH forcing data and its use to assess global and regional reference crop evaporation over land during the twentieth century. *Journal of Hydrometeorology* **12** (5), 823–848. doi: 10.1175/2011JHM1369.1.

WMO 1994 *WMO Guide to Hydrological Practices*, 6th edn. WMO-No. 168, World Meteorological Organization (WMO), Geneva, Switzerland.

Wood, E. F., Lettenmaier, D. P., Liang, X., Lohmann, D., Boone, A., Chang, S., Chen, F., Dai, Y., Dickinson, R. E., Duan, Q., Ek, M., Gusev, Y. M., Habets, F., Irannejad, P., Koster, R., Mitchell, K. E., Nasonova, O. N., Noilhan, J., Schaake, J., Schlosser, A., Shao, Y., Shmakin, A. B., Verseghy, D., Warrach, K., Wetzel, P., Xue, Y., Yang, Z.-L. & Zeng, Q.-C. 1998 The project for intercomparison of land-surface parameterization schemes (PILPS) phase-2(c) Red-Arkansas River basin experiment: 1. Experiment description and summary intercomparisons. *Global and Planetary Change* **19** (1), 115–135. doi: 10.1016/S0921-8181(98)00044-7.

Wu, H., Kimball, J. S., Li, H., Huang, M., Leung, L. R. & Adler, R. F. 2012 A new global river network database for macroscale hydrologic modeling. *Water Resources Research* **48** (9). doi: 10.1029/2012WR012313.

Xu, H. L., Xu, C.-Y., Chen, S. D. & Chen, H. 2016 Similarity and difference of global reanalysis datasets (WFD and APHRODITE) in driving lumped and distributed hydrological models in a humid region of China. *Journal of Hydrology* **542**, 343–356.

First received 26 January 2017; accepted in revised form 2 April 2017. Available online 10 June 2017